

Anomalous Hall effect and two-dimensional Fermi surfaces in the charge-density-wave state of kagome metal RbV_3Sb_5

Lingfei Wang^{§,1}, Wei Zhang^{§,1}, Zheyu Wang^{§,1}, Tsz Fung Poon,¹ Wenyan Wang,¹ Chun Wai Tsang,¹ Jianyu Xie,¹ Xuefeng Zhou,² Yusheng Zhao,² Shanmin Wang,² Kwing To Lai,^{1,3,*} and Swee K. Goh^{1,†}

¹*Department of Physics, The Chinese University of Hong Kong, Shatin, Hong Kong, China*

²*Department of Physics, Southern University of Science and Technology, Shenzhen, Guangdong, China*

³*Shenzhen Research Institute, The Chinese University of Hong Kong, Shatin, Hong Kong, China*

(Dated: February 10, 2023)

AV_3Sb_5 (A=Cs, K, Rb) are recently discovered superconducting systems ($T_c \sim 0.9 - 2.5$ K) in which the vanadium atoms adopt the kagome structure. Intriguingly, these systems enter a charge-density-wave (CDW) phase ($T_{\text{CDW}} \sim 80 - 100$ K), and further evidence shows that the time-reversal symmetry is broken in the CDW phase. Concurrently, the anomalous Hall effect has been observed in KV_3Sb_5 and CsV_3Sb_5 inside the novel CDW phase. Here, we report a comprehensive study of a high-quality RbV_3Sb_5 single crystal with magnetotransport measurements. Our data demonstrate the emergence of anomalous Hall effect in RbV_3Sb_5 when the charge-density-wave state develops. The magnitude of anomalous Hall resistivity at the low temperature limit is comparable to the reported values in KV_3Sb_5 and CsV_3Sb_5 . The magnetoresistance channel further reveals a rich spectrum of quantum oscillation frequencies, many of which have not been reported before. In particular, a large quantum oscillation frequency (2235 T), which occupies $\sim 56\%$ of the Brillouin zone area, has been recorded. For the quantum oscillation frequencies with sufficient signal-to-noise ratio, we further perform field-angle dependent measurements and our data indicate two-dimensional Fermi surfaces in RbV_3Sb_5 . Our results provide indispensable information for understanding the anomalous Hall effect and band structure in kagome metals AV_3Sb_5 .

I. INTRODUCTION

Kagome lattice intrinsically hosts the flat electronic band, van Hove singularities and the Dirac band¹⁻³. Thus, when the charge degree of freedom is enabled, a kagome system provides an important platform to explore both the effect of electronic correlation and topological physics, and a rich variety of phenomena can be expected. The recently discovered kagome metals AV_3Sb_5 (A=K, Rb, Cs), in which the V atoms form a perfect kagome net, are an ideal manifestation of the diverse phenomena this structural class can offer⁴⁻²⁵. Indeed, calculations and experiments have revealed several Dirac-like band crossings near the Fermi energy with a non-zero Z_2 topological invariant^{5,11,26}. Furthermore, these systems exhibit interesting and intertwining electronic phases, including a charge-density-wave (CDW) phase, electronic nematicity as well as superconductivity⁴⁻²⁵.

The CDW phase of AV_3Sb_5 , which sets in at $T_{\text{CDW}} \sim 80 - 100$ K, has been argued to have an unconventional origin. Chiral charge order, the absence of acoustic phonon anomaly, and time-reversal symmetry breaking (TRSB) have been observed in the CDW phase^{8,15,20,27-35}. Below T_{CDW} , a giant anomalous Hall effect (AHE) has been reported in KV_3Sb_5 and CsV_3Sb_5 , supporting the notion of TRSB^{20,21}. Given that the superconductivity, which sets in at $T_c \sim 0.9 - 2.5$ K, arises from this unconventional metallic state, understanding the CDW phase and the phenomena associated with the CDW phase is essential for deepening the understanding of the superconducting state. Further evidence of the nontrivial interplay between the CDW state and superconductivity comes from pressure studies - while T_{CDW}

is suppressed monotonically by pressure, T_c shows an unusual double dome dependence on pressure^{6,7,22,36}.

Although all three AV_3Sb_5 compounds show similar physical properties, CsV_3Sb_5 is currently the most heavily studied, probably because it has the highest T_c . However, both KV_3Sb_5 and RbV_3Sb_5 should also be investigated to build an overall picture for understanding this family of V-based kagome superconductors. For instance, a μSR experiment shows that the superconducting energy gap can be tuned from nodal at ambient pressure to nodeless under pressure in RbV_3Sb_5 and KV_3Sb_5 ³², but this tunability is absent in CsV_3Sb_5 where the gap is found to be nodeless over a large pressure range³⁷. Whether the observed nodal gap is related to TRSB needs to be addressed. However, the anomalous Hall effect (AHE), a signature of TRSB, has not been comprehensively reported in RbV_3Sb_5 , to the best of our knowledge.

Detailed studies of the Fermi surface via quantum oscillations have also been lacking in RbV_3Sb_5 , again in stark contrast to the progress made in CsV_3Sb_5 ^{20,22,26,38-45}. In the pioneering work by Yin *et al.*⁴⁶, only two quantum oscillation frequencies at a single field angle are reported. In particular, these frequencies are rather small - $F_\alpha = 34$ T and $F_\beta = 117$ T, indicating the detection of small Fermi surface sheets. However, much larger frequencies up to 9930 T when the magnetic field is parallel to the c -axis have been reported in CsV_3Sb_5 ⁴⁴. Therefore, it is urgently needed to re-investigate the Fermi surface of RbV_3Sb_5 via quantum oscillations.

In this manuscript, we focus on RbV_3Sb_5 and conduct a series of magnetotransport experiments on high-quality single crystals. We first patch the gap in the

literature by reporting the observation of a large AHE in RbV_3Sb_5 . Next, we analyze the magnetoresistance, uncovering quantum oscillations (the Shubnikov-de Haas (SdH) effect) with 12 frequencies. Notably, the largest frequency detected is 2235 T, nearly 20 times larger than the largest frequency reported by Yin *et al.*⁴⁶. Finally, our field angle dependent data establish that these frequencies are associated with quasi-two-dimensional Fermi surface sheets.

II. METHODS

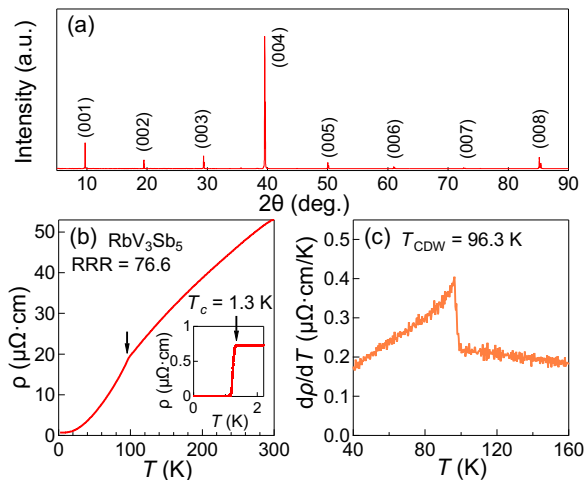


FIG. 1. (a) X-ray diffraction pattern of a RbV_3Sb_5 single crystal showing only (00L) peaks. (b) Temperature dependence of the resistivity of RbV_3Sb_5 under a zero external magnetic field. The RRR is 76.6. The inset displays the superconducting transition starting at 1.3 K. (c) Temperature dependence of $d\rho/dT$, displaying a sharp peak at $T_{\text{CDW}} = 96.3$ K.

Single crystals of RbV_3Sb_5 were synthesized from Rb (ingot, 99.95 %), V (powder, 99.9 %) and Sb (shot, 99.9999 %) using self-flux method similar to Ref. [46]. Raw materials with the molar ratio of Rb:V:Sb = 5.5:7:14 were sealed in a quartz tube. To avoid the possible influence of the ambient environment, all preparation processes were performed in an argon-filled glovebox, before the quartz tube was moved to the furnace for heat treatment. The mixture was first heated to 1000°C with the rate of 20°C/h. After being held at 1000 °C for 24 h, it was cooled to 900°C at 50 °C/h, followed by a further cooling to 400°C at 2 °C/h. The excess flux was removed by distilled water and ethanol. The as-grown single crystals were millimeter-sized shiny plates.

X-ray diffraction (XRD) data were collected at room temperature by using a Rigaku X-ray diffractometer with $\text{CuK}\alpha$ radiation. The chemical compositions were characterized by a JEOL JSM-7800F scanning electron microscope equipped with an Oxford energy-dispersive X-ray

EDX spectrometer.

For magnetotransport measurements, the sample was firstly exfoliated from a bulk crystal and then transferred to a diamond surface pre-patterned with Au/Ti electrodes in a standard six-probe Hall bar configuration. A polydimethylsiloxane (PDMS) film were used to perform the transfer and Dupont 6838 silver paste was used to connect external leads with the electrodes. The transfer process was also performed in the glove box, and in order to protect the sample, we capped the sample with a thin layer (~ 500 nm) of h-BN. The thickness of the thin flakes and h-BN was determined by a dual-beam focused ion beam system (Scios 2 DualBeam by Thermo Scientific). These steps are similar to procedures optimized by us in Refs. 47 and 48.

Low-temperature and high-field measurements were carried out in a commercial Physical Property Measurement System (PPMS) by Quantum Design. A Stanford Research 830 lock-in amplifier was used for Shubnikov-de Haas measurements, while the standard PPMS Resistivity option was used for recording magnetoresistance and Hall effect. The rotator insert option by Quantum Design was used to tilt the angle between magnetic field and the ab plane of the sample. During the rotation, the current direction is kept perpendicular to the magnetic field. A dilution fridge was additionally employed to measure the superconducting transition in RbV_3Sb_5 .

III. RESULTS

Figure 1(a) displays the XRD pattern of an as-grown single crystal of RbV_3Sb_5 . The data can be indexed by the (00L) patterns from the crystal structure of RbV_3Sb_5 (space group: $P6/mmm$) reported in previous studies^{4,46}. This shows that our sample has a preferred orientation, as expected for a single crystal of layered materials. The chemical composition of the single crystal is obtained to be Rb:V:Sb = 0.94:2.86:5 via EDX (see the Supplementary Information), which further confirms the result of XRD in Fig. 1(a).

Figure 1(b) shows the temperature dependence of the electrical resistivity ($\rho(T)$) of our RbV_3Sb_5 sample. The residual resistivity ratio (RRR) (defined as $\rho(300\text{K})/\rho(2\text{K})$) is about 77, currently one of the highest reported values. The $d\rho/dT$ vs. T relation is shown in Fig. 1(c), where an anomaly can be clearly identified at 96.3 K. We associate this anomaly with T_{CDW} , and our value is slightly lower than the reported value for this compound^{46,49,50}.

The availability of high-quality single crystals enables us to investigate the important transport phenomena in RbV_3Sb_5 . We are particularly interested in anomalous Hall effect and quantum oscillations. We have performed Hall measurements over a wide range of temperatures. Figure 2(a) shows the Hall response below T_{CDW} while Fig. 2(b) shows that at temperatures higher than T_{CDW} . The magnetic field (B) is parallel to the c -axis. At

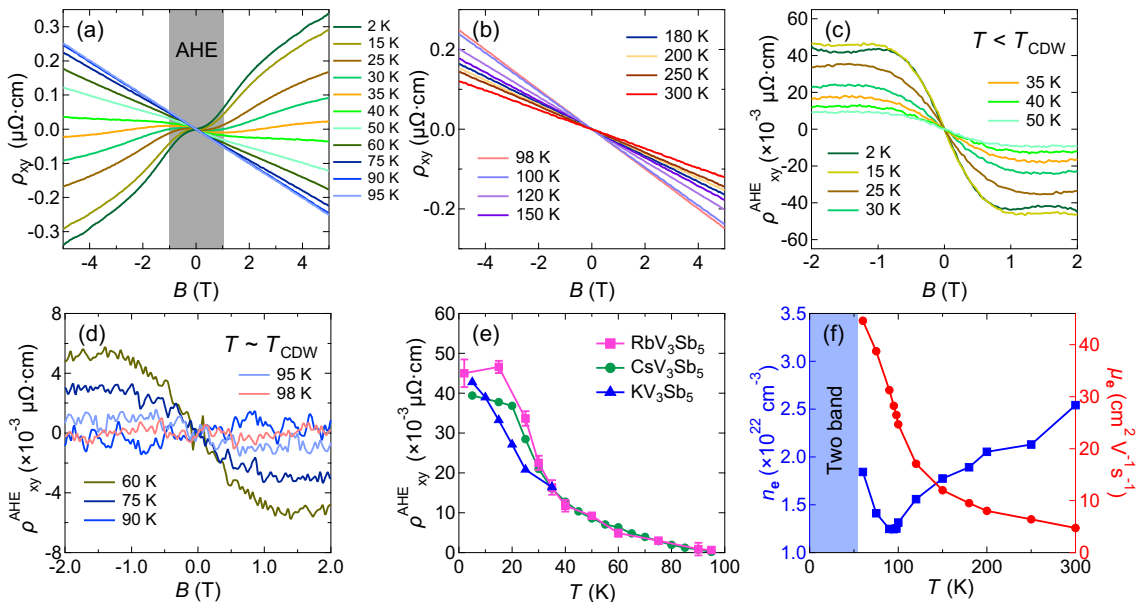


FIG. 2. (a), (b) Field dependence of Hall resistivity at various temperatures. The grey shading area represents the anomalous Hall effect (AHE) observed in the low-field region at all temperatures below T_{CDW} . (c), (d) Anomalous Hall resistivity ρ_{xy}^{AHE} at various temperatures after subtracting the ordinary Hall signal. The AHE shows up for all temperature below T_{CDW} . (e) ρ_{xy}^{AHE} in RbV_3Sb_5 , KV_3Sb_5 and CsV_3Sb_5 as a function of temperature. The data of KV_3Sb_5 and CsV_3Sb_5 are adapted from Refs. [21] and [22], respectively. (f) Temperature dependence of electron carrier density n_e and mobility μ_e in RbV_3Sb_5 extracted from the ordinary Hall signal in the one-band regime.

$T > T_{\text{CDW}}$, the Hall resistivity (ρ_{xy}) is perfectly linear in B , with the slope of $\rho_{xy}(B)$ curves gradually decreases upon cooling. The linearity persists up to ± 14 T, as shown in Fig. S1. At temperatures near T_{CDW} , $\rho_{xy}(B)$ starts to deviate from the linear behavior and an anti-symmetric, sideways “S” shape begins to emerge in the low-field region, as highlighted by the grey shading region in Fig. 2(a). With a further cooling towards the base temperature, the “S”-shaped feature becomes even more pronounced.

The Hall response of RbV_3Sb_5 is reminiscent of the observation in sister compounds KV_3Sb_5 and CsV_3Sb_5 . In particular, the emergence of the low-field “S”-shaped region can be attributed to the development of the anomalous Hall effect on the backdrop of the ordinary Hall effect. To extract the anomalous Hall component ρ_{xy}^{AHE} , we subtract a linear background from the total Hall signals using the data from -2 T to $+2$ T. The slope of the linear background is temperature-dependent, and it is derived from the locally linear region between 1 T and 2 T at all temperatures below T_{CDW} . This analysis results in traces shown in Figs. 2(c) and 2(d). Using the ρ_{xy}^{AHE} at the plateau region as the benchmark, we trace the temperature dependence of the AHE (see Fig. 2(e)). It is worth noticing that the magnitude of ρ_{xy}^{AHE} monotonically decreases with an increasing temperature, and becomes significantly weakened near T_{CDW} . In fact, the disappearance of ρ_{xy}^{AHE} coincides with T_{CDW} , indicating an intimate relationship between the anomalous Hall effect

and the CDW phase. Also included in Fig. 2(e) are ρ_{xy}^{AHE} of CsV_3Sb_5 and KV_3Sb_5 from Refs. 20 and 21. Between ~ 35 K and ~ 95 K, $\rho_{xy}^{\text{AHE}}(T)$ of RbV_3Sb_5 and CsV_3Sb_5 overlap almost perfectly. Furthermore, these data connect smoothly to ρ_{xy}^{AHE} of KV_3Sb_5 near 35 K. Finally, we extract the mobility (μ_e) and the carrier density (n_e) for $\rho_{xy}(B)$ traces that are linear over a wide field range, using a simple single band model. We find that n_e exhibits a minimum right at T_{CDW} while μ_e is significantly enhanced upon cooling across T_{CDW} . These temperature dependence are similar to the observation reported in KV_3Sb_5 .

We now present the second element obtained from our magnetotransport data. In Figs. 3(a) and 3(b), we show the SdH oscillations collected with $B \parallel c$ after removing the background. Two different field ranges are shown: a long field range offers a better view of low-frequency oscillations, while a narrower field range is adopted to display the finer structure in our data due to higher SdH frequencies. Fast Fourier transform (FFT) spectra are shown in Figs. 3(c-f). We detect a rich structure, uncovering at least 12 SdH peaks in the range of between 0 and 3987 T, where 3987 T is the area of the reconstructed Brillouin zone in the k_x - k_y plane expressed as a quantum oscillation frequency. F_α and F_β are consistent with the previous report by Yin *et al.*⁴⁶, but the remaining peaks have never been reported.

In Figs. 3(c-f), the new peaks are marked with red Greek symbols. Following the convention proposed for

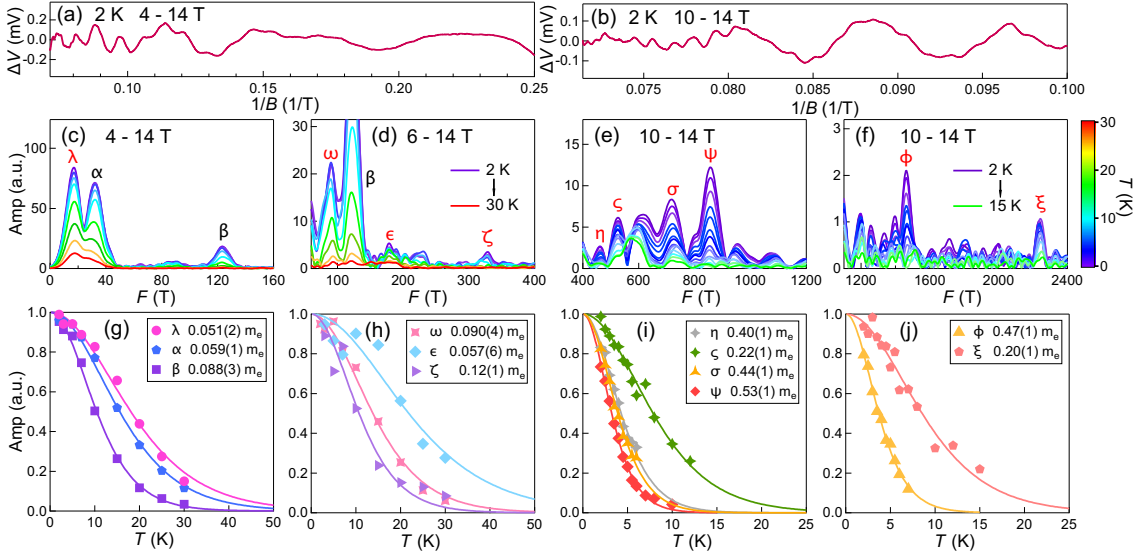


FIG. 3. (a, b) Oscillation signals after removing the background. (c-f) Fast Fourier transform (FFT) spectra in four different ranges: (c) 0-160 T, (d) 60-400 T, (e) 400-1200 T, (f) 1100-2400 T. The field ranges used for FFT analyses are 4-14 T, 6-14 T, 10-14 T and 10-14 T in (c), (d), (e) and (f), respectively. The data were collected at various temperatures ranging from 2 K to 30 K. The peaks are marked in the figures as $\lambda \sim 17$ T, $\alpha \sim 34$ T, $\beta \sim 121$ T, $\omega \sim 91$ T, $\epsilon \sim 178$ T, $\zeta \sim 322$ T, $\eta \sim 461$ T, $\sigma \sim 525$ T, $\psi \sim 716$ T, $\psi \sim 856$ T, $\phi \sim 1461$ T and $\xi \sim 2235$ T. The peaks labelled in red are newly discovered in our findings, while those labelled in black have been reported previously. (g-j) Temperature dependence of FFT amplitude of the peaks obtained in (c-f) and the corresponding Lifshitz-Kosevich fittings. The estimated effective masses are shown in the figures.

CsV₃Sb₅,⁴⁰ we regard the SdH frequencies lower than 500 T as belonging to the ‘low-frequency spectrum’. In the literature of CsV₃Sb₅, low-frequency spectrum has been presented in almost all reports, with excellent consistency. On the other hand, peaks in the mid-frequency spectrum (between 500 T and 2000 T) and the high-frequency spectrum (greater than 2000 T) of CsV₃Sb₅ are absent in many report. In RbV₃Sb₅, our F_α and F_β are similarly in good agreement with the previous report⁴⁶. However, our data additionally reveal peaks in both the mid-frequency to the high-frequency spectra (Figs. 3(e) and (f)). The largest frequency (F_ξ) reaches 2235 T. These frequencies indicate that RbV₃Sb₅ in the CDW phase hosts multiple Fermi surface sheets, and the largest cyclotron orbit encloses an area that is $\sim 56\%$ of the Brillouin zone area.

Following the Lifshitz-Kosevich theory, we analyze the temperature dependence of the oscillation amplitudes using the thermal damping factor $R_T = X/\sinh X$ with $X = 14.693m^*T/B$, from which we can calculate the cyclotron effective mass m^* of the peaks marked by the Greek symbols. As shown in Figs. 3(g-j), m^* of the low-frequency peaks (λ , α , β , ω , ϵ and ζ) are relatively small, all less than $0.1m_e$ except for ζ , which is slightly higher ($0.12m_e$). However, m^* of the mid-frequency and the high-frequency peaks are comparatively larger, all greater than $0.2m_e$ with ψ having the largest value of $0.53m_e$. Finally, we note our observation that some peaks shift at higher temperatures. We attribute this phenomenon to noise contamination. Indeed, this happens

to weak peaks that are close to the noise floor, and they are excluded from our analysis. For instance, only the data between 2 K and 6 K are included for m^* analysis for η and σ (see Figs. 3(e) and 3(i)).

We now explore the dimensionality of the Fermi surface. Figure 4 shows the FFT spectra at 2 K for selected magnetic field angles θ , where $\theta = 0^\circ$ corresponds to $B//c$ and B is rotated towards the sample ab -plane with an increasing θ . The intensities of all peaks gradually decrease with an increasing angle, especially for the peaks with relatively high frequencies (> 500 T). However, we are able to follow several stronger peaks to higher angles. F_α , F_β and F_ω , which are the more intense peaks, can be traced with ease to $\sim 70^\circ$. For higher frequencies F_ζ , F_ψ and F_ξ , the signals are weaker but we are able to follow their angular evolution to $\sim 35^\circ$. All these frequencies display $1/\cos\theta$ dependence (Fig. 4), indicating the quasi-two-dimensional nature of RbV₃Sb₅. Additionally, we recorded a peak with $F(0^\circ) = 212$ T, which also exhibits a $1/\cos\theta$ dependence (see the curves labelled by asterisk in Figs. 4(b) and (d)). However, the temperature dependence of this peak does not conform to the description of R_T .

The total oscillatory signals can be decomposed into constituent components, with the i^{th} component taking the form of^{26,51,52}

$$\Delta\rho_{xx}^i \sim A_i \cos\left(2\pi\left(\frac{F_i}{B} + \gamma_i - \delta_i\right)\right), \quad (1)$$

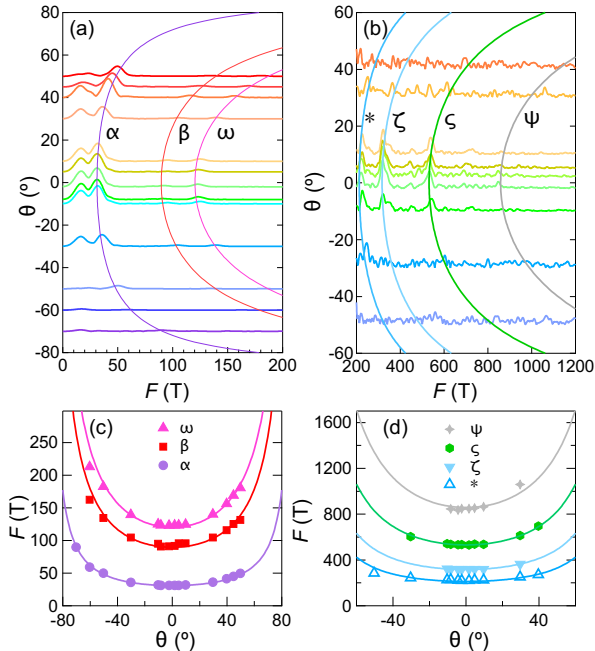


FIG. 4. FFT spectra of SdH oscillations at different field angles (θ) for frequencies ranging from (a) 0 to 200 T and (b) 200 T to 1200 T. All peaks shift towards higher frequencies as θ increases. (c, d) Angular dependence of different oscillation frequencies. The curves in all panels are the fittings based on the formula $F(\theta) = F(0^\circ)/\cos\theta$.

where A_i is the oscillation amplitude that depends on the relevant damping factors. For the phase factor, $\gamma_i = 1/2 - \phi_{B_i}/2\pi$ where ϕ_{B_i} is the Berry phase⁵³. δ_i depends on the dimensionality of the Fermi surface, and it is equal to 0 or $\pm\frac{1}{8}$ when the Fermi surface is two-dimensional or three-dimensional, respectively⁵⁴. We construct a Landau level (LL) fan diagram for β based on the data at 2 K, as β is the easiest component to isolate with a digital high-pass filter. The high-pass filter removed the contribution from λ and α , making β the dominant component (the components with $F > F_\beta$ makes negligible contribution.) Figure 5(a) shows the filtered signal and the inset is the corresponding FFT spectrum, showing the dominance of β band. At ± 14 T, $\rho_{xx}/|\rho_{xy}| \sim 5$ (shown in Fig. S1) and this ratio significantly increases with a decreasing external field. As a result, $\sigma_{xx} = \frac{\rho_{xx}}{\rho_{xx}^2 + \rho_{xy}^2} \approx \frac{1}{\rho_{xx}}$, showing that ρ_{xx} reaches a local minimum when σ_{xx} reaches a local maximum and vice versa. Our oscillatory voltage ΔV is proportional to oscillatory resistivity $\Delta\rho_{xx}$. Thus, the LL integer indices N can be safely assigned to the local maxima of the signal while the LL half-integer indices $N + 1/2$ are assigned to the minima, as shown in Fig. 5(b). We then perform the linear fitting of N as a function of $1/B$. The fitted slope is 121 T, identical to the frequency of β , suggesting the

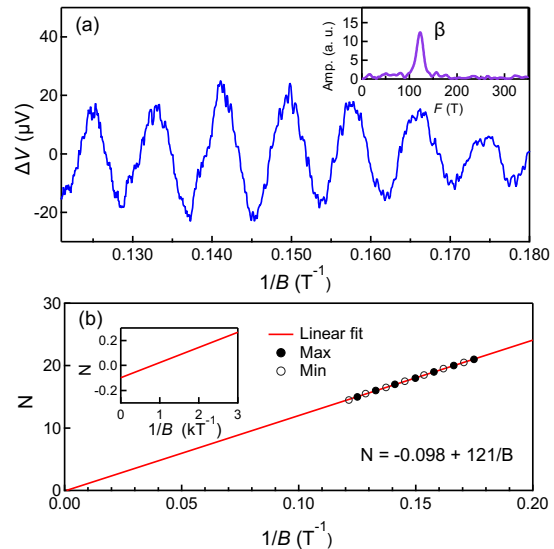


FIG. 5. (a) The oscillatory signal ΔV (proportional to oscillatory ρ_{xx}) of F_β as a function of inverse magnetic field B^{-1} . A high pass digital filter was used to eliminate the intense λ and α signals. The inset shows the FFT spectrum of the filtered signal. (b) Landau level fan diagram analysis of F_β constructed with the filtered signal shown in (a). The closed circles denote integer indices while the open ones indicate half-integer indices. The red line is a linear fit of the data. The inset shows an enlarged view near the origin.

reliability of our analysis. The intercept on the LL index axis is -0.098 . Considering the two-dimensional nature of β as shown in Fig. 4(a), the value of δ_β should be zero. Finally we can obtain $\phi_B = 2\pi \times (-0.098) = -0.196\pi$. This value is close to 0, indicating a trivial Berry phase for β . This result shows that β band does not contribute to σ_{xx}^{AHE} intrinsically, while the topology of other bands should attract further study.

IV. DISCUSSION

The fact that RbV_3Sb_5 is also able to support the giant anomalous Hall effect brings new insights to the study of AV_3Sb_5 compounds. One remarkable feature deserving further investigation is the good agreement across all three AV_3Sb_5 compounds (see Fig. 2(e)), considering the fact that these measurements were collected on different crystals by independent groups. This suggests similar origins of AHE. Besides, a similar scaling relation between σ_{xy}^{AHE} and σ_{xx} observed in RbV_3Sb_5 and the other two compounds also supports this opinion. As plotted in Fig. S2, we can identify a region where $\sigma_{xy}^{\text{AHE}} \propto \sigma_{xx}^2$ when σ_{xx} exceeds $\sim 2 \times 10^5 \Omega^{-1}\text{cm}^{-1}$.

Judging from the magnitude of σ_{xx} , skew scattering has been put forward to explain the observed AHE in CsV_3Sb_5 and KV_3Sb_5 (Refs. 20, 21, and 55). However,

the mechanism giving rise to skew scattering is still under debate. In KV_3Sb_5 , it is attributed to a spin cluster model with an extra spin-orbit coupling. In CsV_3Sb_5 , tiny amounts of paramagnetic impurities could cause the skew scattering. However, as pointed out by Yu *et al.*²⁰, it is not clear if a very low level of paramagnetic impurities is sufficient to cause the large AHE observed. When it comes to RbV_3Sb_5 , skew scattering is likely to be a dominant mechanism, as the region of σ_{xx} where the large AHE is observed is similar to KV_3Sb_5 and CsV_3Sb_5 . However, the source of the skew scattering requires more studies. Nevertheless, the possibility of an intrinsic mechanism giving rise to the AHE should still be investigated, as TRSB has been observed in the CDW state without the external magnetic field. All the evidence indicates a topological band structure could be a potential source of intrinsic anomalous Hall effect in AV_3Sb_5 . Unfortunately, our LL fan diagram analysis only covers β frequency. Further study on other frequencies is urgently needed.

The observation of the AHE in the CDW state in all three AV_3Sb_5 compounds clearly highlights the unconventional nature of this phase, demonstrating the need to understand the CDW state. In this regard, the Fermi surface of these compounds in the CDW state is an important gateway to achieve this understanding. Density functional theory (DFT) calculations performed on CsV_3Sb_5 assuming either a ‘star-of-David’ (SoD) or a trihexagonal (TrH) deformation, the so-called $2 \times 2 \times 1$ distortion, can not explain our rich spectrum in RbV_3Sb_5 . It has been pointed that additional interlayer complexity that involves both SoD and TrH can introduce new quantum oscillation frequencies^{40,45}. Therefore, future

DFT calculations on RbV_3Sb_5 taking into account various stacking arrangements of SD and ISD will shed light on this issue, and our quantum oscillation data will potentially be useful for settling the superlattice structure in the CDW phase of RbV_3Sb_5 .

V. CONCLUSIONS

To summarize, we have synthesised high-quality single crystals of RbV_3Sb_5 and conducted the magnetotransport measurements up to 14 T. Close to the zero field, we detect the emergence of the anomalous Hall effect, while at high fields, we unravel a rich quantum oscillation spectrum. The magnitude of the anomalous Hall resistivity is large, on par with the observation in the sister compounds CsV_3Sb_5 ²⁰ and KV_3Sb_5 ²¹, highlighting AV_3Sb_5 as a suitable platform to explore the physics of anomalous Hall resistivity. Regarding quantum oscillations, we report 12 frequencies, with the largest frequency having a value of 2235 T. Angular dependencies of some of these frequencies show that they originate from two-dimensional Fermi surfaces, consistent with the layered nature of RbV_3Sb_5 .

ACKNOWLEDGMENTS

This work was supported by Research Grants Council of Hong Kong (CUHK 14301020, CUHK 14300722, ACUHK402/19), CUHK Direct Grant (4053461, 4053408, 4053528, 4053463), the National Natural Science Foundation of China (12104384, 12174175) and the Shenzhen Basic Research Fund (JCYJ20190809173213150).

[‡]L.W., W.Z. and Z.W. contributed equally to this work.

* ktlai@phy.cuhk.edu.hk

† skgoh@cuhk.edu.hk

¹ M. L. Kiesel and R. Thomale, “Sublattice interference in the kagome Hubbard model,” *Phys. Rev. B* **86**, 121105 (2012).

² M. L. Kiesel, C. Platt, and R. Thomale, “Unconventional fermi surface instabilities in the kagome Hubbard model,” *Phys. Rev. Lett.* **110**, 126405 (2013).

³ W.-S. Wang, Z.-Z. Li, Y.-Y. Xiang, and Q.-H. Wang, “Competing electronic orders on kagome lattices at van Hove filling,” *Phys. Rev. B* **87**, 115135 (2013).

⁴ B. R. Ortiz, L. C. Gomes, J. R. Morey, M. Winiarski, M. Bordelon, J. S. Mangum, I. W. H. Oswald, J. A. Rodriguez-Rivera, J. R. Neilson, S. D. Wilson, E. Ertekin, T. M. McQueen, and E. S. Toberer, “New kagome prototype materials: discovery of KV_3Sb_5 , RbV_3Sb_5 , and CsV_3Sb_5 ,” *Phys. Rev. Mater.* **3**, 094407 (2019).

⁵ B. R. Ortiz, S. M. L. Teicher, Y. Hu, J. L. Zuo, P. M. Sarte, E. C. Schueller, A. M. M. Abeykoon, M. J. Krogstad, S. Rosenkranz, R. Osborn, R. Seshadri, L. Balents, J. He, and S. D. Wilson, “ CsV_3Sb_5 : A \mathbb{Z}_2 topological kagome metal with a superconducting ground state,” *Phys. Rev. Lett.* **125**, 247002 (2020).

⁶ F. Du, S. Luo, B. R. Ortiz, Y. Chen, W. Duan, D. Zhang, X. Lu, S. D. Wilson, Y. Song, and H. Yuan, “Pressure-induced double superconducting domes and charge instability in the kagome metal KV_3Sb_5 ,” *Phys. Rev. B* **103**, L220504 (2021).

⁷ K. Y. Chen, N. N. Wang, Q. W. Yin, Y. H. Gu, K. Jiang, Z. J. Tu, C. S. Gong, Y. Uwatoko, J. P. Sun, H. C. Lei, J. P. Hu, and J.-G. Cheng, “Double superconducting dome and triple enhancement of T_c in the kagome superconductor CsV_3Sb_5 under high pressure,” *Phys. Rev. Lett.* **126**, 247001 (2021).

⁸ H. Li, T. T. Zhang, T. Yilmaz, Y. Y. Pai, C. E. Marvinney, A. Said, Q. W. Yin, C. S. Gong, Z. J. Tu, E. Vescovo, C. S. Nelson, R. G. Moore, S. Murakami, H. C. Lei, H. N. Lee, B. J. Lawrie, and H. Miao, “Observation of unconventional charge density wave without acoustic phonon anomaly in kagome superconductors AV_3Sb_5 ($A = \text{Rb}, \text{Cs}$),” *Phys. Rev. X* **11**, 031050 (2021).

⁹ Z. Liang, X. Hou, F. Zhang, W. Ma, P. Wu, Z. Zhang, F. Yu, J.-J. Ying, K. Jiang, L. Shan, Z. Wang, and X.-H. Chen, “Three-dimensional charge density wave and surface-dependent vortex-core states in a kagome superconductor CsV_3Sb_5 ,” *Phys. Rev. X* **11**, 031026 (2021).

- ¹⁰ H. Zhao, H. Li, B. R. Ortiz, S. M. L. Teicher, T. Park, M. Ye, Z. Wang, L. Balents, S. D. Wilson, and I. Zeljkovic, “Cascade of correlated electron states in the kagome superconductor CsV_3Sb_5 ,” *Nature* **599**, 216 (2021).
- ¹¹ Z. Liu, N. Zhao, Q. Yin, C. Gong, Z. Tu, M. Li, W. Song, Z. Liu, D. Shen, Y. Huang, K. Liu, H. Lei, and S. Wang, “Charge-density-wave-induced bands renormalization and energy gaps in a kagome superconductor RbV_3Sb_5 ,” *Phys. Rev. X* **11**, 041010 (2021).
- ¹² Y. Hu, S. M. L. Teicher, B. R. Ortiz, Y. Luo, S. Peng, L. Huai, J. Z. Ma, N. C. Plumb, S. D. Wilson, J. F. He, and M. Shi, “Charge-order-assisted topological surface states and flat bands in the kagome superconductor CsV_3Sb_5 ,” *Sci. Bull.* **67**, 495 (2022).
- ¹³ E. Uykur, B. R. Ortiz, S. D. Wilson, M. Dressel, and A. A. Tsirlin, “Optical detection of charge-density-wave instability in the non-magnetic kagome metal KV_3Sb_5 ,” *npj Quantum Mater.* **7**, 16 (2022).
- ¹⁴ X. Zhou, Y. Li, X. Fan, J. Hao, Y. Dai, Z. Wang, Y. Yao, and H.-H. Wen, “Origin of charge density wave in the kagome metal CsV_3Sb_5 as revealed by optical spectroscopy,” *Phys. Rev. B* **104**, L041101 (2021).
- ¹⁵ Y.-X. Jiang, J.-X. Yin, M. M. Denner, N. Shumiya, B. R. Ortiz, G. Xu, Z. Guguchia, J. He, M. S. Hossain, X. Liu, J. Ruff, L. Kautzsch, S. S. Zhang, G. Chang, I. Belopolski, Q. Zhang, T. A. Cochran, D. Multer, M. Litskevich, Z.-J. Cheng, X. P. Yang, Z. Wang, R. Thomale, T. Neupert, S. D. Wilson, and M. Z. Hasan, “Unconventional chiral charge order in kagome superconductor KV_3Sb_5 ,” *Nat. Mater.* **20**, 1353 (2021).
- ¹⁶ M. Kang, S. Fang, J.-K. Kim, B. R. Ortiz, S. H. Ryu, J. Kim, J. Yoo, G. Sangiovanni, D. Di Sante, B.-G. Park, C. Jozwiak, A. Bostwick, E. Rotenberg, E. Kaxiras, S. D. Wilson, J.-H. Park, and R. Comin, “Twofold van Hove singularity and origin of charge order in topological kagome superconductor CsV_3Sb_5 ,” *Nat. Phys.* **18**, 301 (2022).
- ¹⁷ M. Kang, S. Fang, J. Yoo, B. R. Ortiz, Y. Oey, S. H. Ryu, J. Kim, C. Jozwiak, A. Bostwick, E. Rotenberg, E. Kaxiras, J. Checkelsky, S. D. Wilson, J.-H. Park, and R. Comin, “Microscopic structure of three-dimensional charge order in kagome superconductor AV_3Sb_5 and its tunability,” *arXiv:2202.01902* (2022).
- ¹⁸ S. Wu, B. R. Ortiz, H. Tan, S. D. Wilson, B. Yan, T. Birol, and G. Blumberg, “Charge density wave order in the kagome metal AV_3Sb_5 ($A = \text{Cs}, \text{Rb}, \text{K}$),” *Phys. Rev. B* **105**, 155106 (2022).
- ¹⁹ R. Lou, A. Fedorov, Q. Yin, A. Kuibarov, Z. Tu, C. Gong, E. F. Schwier, B. Büchner, H. Lei, and S. Borisenko, “Charge-density-wave-induced peak-dip-hump structure and the multiband superconductivity in a kagome superconductor CsV_3Sb_5 ,” *Phys. Rev. Lett.* **128**, 036402 (2022).
- ²⁰ F. H. Yu, T. Wu, Z. Y. Wang, B. Lei, W. Z. Zhuo, J. J. Ying, and X. H. Chen, “Concurrence of anomalous Hall effect and charge density wave in a superconducting topological kagome metal,” *Phys. Rev. B* **104**, L041103 (2021).
- ²¹ S.-Y. Yang, Y. Wang, B. R. Ortiz, D. Liu, J. Gayles, E. Derunova, R. Gonzalez-Hernandez, L. Šmejkal, Y. Chen, S. S. P. Parkin, S. D. Wilson, E. S. Toberer, T. McQueen, and M. N. Ali, “Giant, unconventional anomalous Hall effect in the metallic frustrated magnet candidate, KV_3Sb_5 ,” *Sci. Adv.* **6**, eabb6003 (2020).
- ²² F. Yu, D. Ma, W. Zhuo, S. Liu, X. Wen, B. Lei, J. Ying, and X. Chen, “Unusual competition of superconductivity and charge-density-wave state in a compressed topological kagome metal,” *Nat. Commun.* **12**, 3645 (2021).
- ²³ D. Wulferding, S. Lee, Y. Choi, Q. Yin, Z. Tu, C. Gong, H. Lei, S. Yousuf, J. Song, H. Lee, *et al.*, “Emergent nematicity and intrinsic versus extrinsic electronic scattering processes in the kagome metal CsV_3Sb_5 ,” *Phys. Rev. Res.* **4**, 023215 (2022).
- ²⁴ Z. Jiang, H. Ma, W. Xia, Q. Xiao, Z. Liu, Z. Liu, Y. Yang, J. Ding, Z. Huang, J. Liu, *et al.*, “Observation of electronic nematicity driven by three-dimensional charge density wave in kagome lattice KV_3Sb_5 ,” *arXiv:2208.01499* (2022).
- ²⁵ L. Nie, K. Sun, W. Ma, D. Song, L. Zheng, Z. Liang, P. Wu, F. Yu, J. Li, M. Shan, *et al.*, “Charge-density-wave-driven electronic nematicity in a kagome superconductor,” *Nature* **604**, 59 (2022).
- ²⁶ Y. Fu, N. Zhao, Z. Chen, Q. Yin, Z. Tu, C. Gong, C. Xi, X. Zhu, Y. Sun, K. Liu, and H. Lei, “Quantum transport evidence of topological band structures of kagome superconductor CsV_3Sb_5 ,” *Phys. Rev. Lett.* **127**, 207002 (2021).
- ²⁷ X. Feng, K. Jiang, Z. Wang, and J. Hu, “Chiral flux phase in the kagome superconductor AV_3Sb_5 ,” *Sci. Bull.* **66**, 1384 (2021).
- ²⁸ L. Yu, C. Wang, Y. Zhang, M. Sander, S. Ni, Z. Lu, S. Ma, Z. Wang, Z. Zhao, H. Chen, K. Jiang, Y. Zhang, H. Yang, F. Zhou, X. Dong, S. L. Johnson, M. J. Graf, J. Hu, H.-J. Gao, and Z. Zhao, “Evidence of a hidden flux phase in the topological kagome metal CsV_3Sb_5 ,” *arXiv:2107.10714* (2021).
- ²⁹ Y. Hu, S. Yamane, G. Mattoni, K. Yada, K. Obata, Y. Li, Y. Yao, Z. Wang, J. Wang, C. Farhang, *et al.*, “Time-reversal symmetry breaking in charge density wave of CsV_3Sb_5 detected by polar kerr effect,” *arXiv:2208.08036* (2022).
- ³⁰ C. Mielke III, D. Das, J. X. Yin, H. Liu, R. Gupta, Y. X. Jiang, M. Medarde, X. Wu, H. C. Lei, J. Chang, P. Dai, Q. Si, H. Miao, R. Thomale, T. Neupert, Y. Shi, R. Khasanov, M. Z. Hasan, H. Luetkens, and Z. Guguchia, “Time-reversal symmetry-breaking charge order in a kagome superconductor,” *Nature* **602**, 245 (2022).
- ³¹ R. Khasanov, D. Das, R. Gupta, C. Mielke III, M. Elender, Q. Yin, Z. Tu, C. Gong, H. Lei, E. T. Ritz, *et al.*, “Time-reversal symmetry broken by charge order in CsV_3Sb_5 ,” *Phys. Rev. Res.* **4**, 023244 (2022).
- ³² Z. Guguchia, C. Mielke, D. Das, R. Gupta, J. X. Yin, H. Liu, Q. Yin, M. H. Christensen, Z. Tu, C. Gong, N. Shumiya, T. Gamsakhurdashvili, M. Elender, P. Dai, A. Amato, Y. Shi, H. C. Lei, R. M. Fernandes, M. Z. Hasan, H. Luetkens, and R. Khasanov, “Tunable nodal kagome superconductivity in charge ordered RbV_3Sb_5 ,” *arXiv:2202.07713* (2022).
- ³³ E. M. Kenney, B. R. Ortiz, C. Wang, S. D. Wilson, and M. J. Graf, “Absence of local moments in the kagome metal KV_3Sb_5 as determined by muon spin spectroscopy,” *Journal of Physics: Condensed Matter* **33**, 235801 (2021).
- ³⁴ B. R. Ortiz, P. M. Sarte, E. M. Kenney, M. J. Graf, S. M. L. Teicher, R. Seshadri, and S. D. Wilson, “Superconductivity in the \mathbb{Z}_2 kagome metal KV_3Sb_5 ,” *Phys. Rev. Mater.* **5**, 034801 (2021).
- ³⁵ H. Luo, Q. Gao, H. Liu, Y. Gu, D. Wu, C. Yi, J. Jia, S. Wu, X. Luo, Y. Xu, L. Zhao, Q. Wang, H. Mao, G. Liu, Z. Zhu, Y. Shi, K. Jiang, J. Hu, Z. Xu, and X. J. Zhou, “Electronic nature of charge density wave and electron-phonon coupling in kagome superconductor KV_3Sb_5 ,” *Na-*

- ture Communications **13**, 273 (2022).
- ³⁶ N. N. Wang, K. Y. Chen, Q. W. Yin, Y. N. N. Ma, B. Y. Pan, X. Yang, X. Y. Ji, S. L. Wu, P. F. Shan, S. X. Xu, Z. J. Tu, C. S. Gong, G. T. Liu, G. Li, Y. Uwatoko, X. L. Dong, H. C. Lei, J. P. Sun, and J.-G. Cheng, “Competition between charge-density-wave and superconductivity in the kagome metal RbV_3Sb_5 ,” *Phys. Rev. Res.* **3**, 043018 (2021).
- ³⁷ R. Gupta, D. Das, C. Mielke, E. T. Ritz, F. Hotz, Q. Yin, Z. Tu, C. Gong, H. Lei, T. Birol, R. M. Fernandes, Z. Guguchia, H. Luetkens, and R. Khasanov, “Two types of charge order with distinct interplay with superconductivity in the kagome material CsV_3Sb_5 ,” *Commun. Phys.* **5**, 232 (2022).
- ³⁸ B. R. Ortiz, S. M. Teicher, L. Kautzsch, P. M. Sarte, N. Ratcliff, J. Harter, J. P. Ruff, R. Seshadri, and S. D. Wilson, “Fermi surface mapping and the nature of charge-density-wave order in the kagome superconductor CsV_3Sb_5 ,” *Phys. Rev. X* **11**, 041030 (2021).
- ³⁹ Y. Gan, W. Xia, L. Zhang, K. Yang, X. Mi, A. Wang, Y. Chai, Y. Guo, X. Zhou, and M. He, “Magneto-Seebeck effect and ambipolar Nernst effect in the CsV_3Sb_5 superconductor,” *Phys. Rev. B* **104**, L180508 (2021).
- ⁴⁰ W. Zhang, L. Wang, C. W. Tsang, X. Liu, J. Xie, W. C. Yu, K. T. Lai, and S. K. Goh, “Emergence of large quantum oscillation frequencies in thin flakes of the kagome superconductor CsV_3Sb_5 ,” *Phys. Rev. B* **106**, 195103 (2022).
- ⁴¹ D. Chen, B. He, M. Yao, Y. Pan, H. Lin, W. Schnelle, Y. Sun, J. Gooth, L. Taillefer, and C. Felser, “Anomalous thermoelectric effects and quantum oscillations in the kagome metal CsV_3Sb_5 ,” *Phys. Rev. B* **105**, L201109 (2022).
- ⁴² X. Huang, C. Guo, C. Putzke, M. Gutierrez-Amigo, Y. Sun, M. G. Vergniory, I. Errea, D. Chen, C. Felser, and P. J. W. Moll, “Three-dimensional fermi surfaces from charge order in layered CsV_3Sb_5 ,” *Phys. Rev. B* **106**, 064510 (2022).
- ⁴³ K. Shrestha, R. Chapai, B. K. Pokharel, D. Miertschin, T. Nguyen, X. Zhou, D. Y. Chung, M. G. Kanatzidis, J. F. Mitchell, U. Welp, D. Popović, D. E. Graf, B. Lorenz, and W. K. Kwok, “Nontrivial Fermi surface topology of the kagome superconductor CsV_3Sb_5 probed by de Haas–van Alphen oscillations,” *Phys. Rev. B* **105**, 024508 (2022).
- ⁴⁴ R. Chapai, M. Leroux, V. Oliviero, D. Vignolles, M. Smylie, D. Chung, M. Kanatzidis, W.-K. Kwok, J. Mitchell, and U. Welp, “Magnetic breakdown and topology in the kagome superconductor CsV_3Sb_5 under high magnetic field,” arXiv:2208.05523 (2022).
- ⁴⁵ C. Broyles, D. Graf, H. Yang, X. Dong, H. Gao, and S. Ran, “Effect of the interlayer ordering on the Fermi surface of kagome superconductor CsV_3Sb_5 revealed by quantum oscillations,” *Phys. Rev. Lett.* **129**, 157001 (2022).
- ⁴⁶ Q. Yin, Z. Tu, C. Gong, Y. Fu, S. Yan, and H. Lei, “Superconductivity and normal-state properties of kagome metal RbV_3Sb_5 single crystals,” *Chin. Phys. Lett.* **38**, 037403 (2021).
- ⁴⁷ J. Xie, X. Liu, W. Zhang, S. M. Wong, X. Zhou, Y. Zhao, S. Wang, K. T. Lai, and S. K. Goh, “Fragile pressure-induced magnetism in FeSe superconductors with a thickness reduction,” *Nano Lett.* **21**, 9310 (2021).
- ⁴⁸ C.-h. Ku, X. Liu, J. Xie, W. Zhang, S. T. Lam, Y. Chen, X. Zhou, Y. Zhao, S. Wang, S. Yang, et al., “Patterned diamond anvils prepared via laser writing for electrical transport measurements of thin quantum materials under pressure,” *Rev. Sci. Instrum.* **93**, 083912 (2022).
- ⁴⁹ Q. Wang, P. Kong, W. Shi, C. Pei, C. Wen, L. Gao, Y. Zhao, Q. Yin, Y. Wu, G. Li, H. Lei, J. Li, Y. Chen, S. Yan, and Y. Qi, “Charge density wave orders and enhanced superconductivity under pressure in the kagome metal CsV_3Sb_5 ,” *Adv. Mater.* **33**, 2102813 (2021).
- ⁵⁰ S. Cho, H. Ma, W. Xia, Y. Yang, Z. Liu, Z. Huang, Z. Jiang, X. Lu, J. Liu, Z. Liu, J. Li, J. Wang, Y. Liu, J. Jia, Y. Guo, J. Liu, and D. Shen, “Emergence of new van hove singularities in the charge density wave state of a topological kagome metal RbV_3Sb_5 ,” *Phys. Rev. Lett.* **127**, 236401 (2021).
- ⁵¹ J. Hu, Z. Tang, J. Liu, X. Liu, Y. Zhu, D. Graf, K. Myhro, S. Tran, C. N. Lau, J. Wei, and Z. Mao, “Evidence of topological nodal-line fermions in ZrSiSe and ZrSiTe ,” *Phys. Rev. Lett.* **117**, 016602 (2016).
- ⁵² D. Shoenberg, *Magnetic Oscillations in Metals*, Cambridge Monographs on Physics (Cambridge University Press, 1984).
- ⁵³ G. P. Mikitik and Y. V. Sharlai, “Manifestation of berry’s phase in metal physics,” *Phys. Rev. Lett.* **82**, 2147 (1999).
- ⁵⁴ F.-X. Xiang, X.-L. Wang, M. Veldhorst, S.-X. Dou, and M. S. Fuhrer, “Observation of topological transition of fermi surface from a spindle torus to a torus in bulk Rashba spin-split BiTeCl ,” *Phys. Rev. B* **92**, 035123 (2015).
- ⁵⁵ N. Nagaosa, J. Sinova, S. Onoda, A. H. MacDonald, and N. P. Ong, “Anomalous hall effect,” *Rev. Mod. Phys.* **82**, 1539 (2010).